Multimode Hong-Ou-Mandel Interference

S. P. Walborn,* A. N. de Oliveira, S. Pádua, and C. H. Monken
Universidade Federal de Minas Gerais, Caixa Postal 702, Belo Horizonte, MG 30123-970, Brazil
(Received 25 September 2002; published 8 April 2003)

We consider multimode two-photon interference at a beam splitter by photons created by spontaneous parametric down-conversion. The resulting interference pattern is shown to depend upon the transverse spatial symmetry of the pump beam. In an experiment, we employ the first-order Hermite-Gaussian modes in order to show that, by manipulating the pump beam, one can control the resulting two-photon interference behavior. We expect these results to play an important role in the engineering of quantum states of light for use in quantum information processing and quantum imaging.

DOI: 10.1103/PhysRevLett.90.143601 PACS numbers: 42.50.Ar, 03.67.–a

Two-photon interference at a beam splitter was first demonstrated by Hong, Ou, and Mandel (HOM) [1]. It has since been utilized in quantum tests of nonlocality [2] as well as many optical implementations of quantum information protocol such as Bell-state measurements [3,4] and may be used to construct quantum-optical logic gates [5,6]. To date, however, most experiments utilizing HOM-type interference consider an ideal monomode situation. In this Letter, we consider multimode two-photon interference of photon pairs created by spontaneous parametric down-conversion (SPDC). We show how the transverse amplitude profile of the pump beam in SPDC determines whether the down-converted fields interfere constructively or destructively. We present our experiment and conclude by noting the relevance of these results to quantum-optical information processing.

Consider the HOM interferometer shown in Fig. 1, in which two photons generated by SPDC are reflected onto opposite sides of a beam splitter. We assume that paths s and i are equal. Here we work in the monochromatic and paraxial approximations. This is justified by the use of narrow bandwidth interference filters (centered at $2\lambda_p$, where λ_p is the pump field wavelength) and small collection apertures in the experimental setup (see Fig. 2). Under such conditions, we have $k_s = k_i = K/2$, where k_s and k_i are the magnitudes of the wave vectors of the down-converted fields and K is the magnitude of the pump field wave vector. Following [8,9], the two-photon quantum state generated by noncolinear SPDC is then

$$|\psi\rangle_{\mathrm{SPDC}} = C_1|\mathrm{VAC}\rangle + C_2|\psi\rangle, \tag{1}$$

where

$$|\psi\rangle = \sum_{\sigma_s,\sigma_i} C_{\sigma_s,\sigma_i} \iint_D d\mathbf{q}_s d\mathbf{q}_i \Phi(\mathbf{q}_s, \mathbf{q}_i)|\mathbf{q}_s, \sigma_s\rangle_s|\mathbf{q}_i, \sigma_i\rangle_i. \tag{2}$$

The coefficients C_1 and C_2 are such that $|C_2| \ll |C_1|$. C_2 depends on the crystal length, the nonlinearity coefficient, and the magnitude of the pump field, among other factors. The kets $|\mathbf{q}_j, \sigma_j\rangle$ represent Fock states labeled by the transverse component $\mathbf{q}_j$ of the wave vector $\mathbf{k}_j$ and by the polarization σ_j of the mode $j = s$ or i. The polarization state of the down-converted photon pair is defined by the coefficients C_{σ_s,σ_i}. When the crystal output angles of s and i are small, the function $\Phi(\mathbf{q}_s, \mathbf{q}_i)$, which can be regarded as the normalized angular spectrum of the two-photon field [9], is given by

$$\Phi(\mathbf{q}_s, \mathbf{q}_i) = \frac{1}{\pi}\sqrt{\frac{2L}{K}}\upsilon(\mathbf{q}_s + \mathbf{q}_i)\mathrm{sinc}\left(\frac{L|\mathbf{q}_s - \mathbf{q}_i|^2}{4K}\right), \tag{3}$$

where $\upsilon(\mathbf{q})$ is the normalized angular spectrum of the pump beam, L is the length of the nonlinear crystal in the z direction, K is the magnitude of the pump field wave vector defined above, and $\mathrm{sinc}(x) = \sin(x)/x$. The integration domain D is, in principle, defined by the conditions $q_s^2 \le k_s^2$ and $q_i^2 \le k_i^2$. However, in most experimental conditions, the domain in which $\Phi(\mathbf{q}_s, \mathbf{q}_i)$ is appreciable is much smaller. Equations (2) and (3) include the wave vectors inside the nonlinear birefringent crystal, which, upon propagation through the crystal, may suffer transverse and longitudinal walk-off effects, as well as refraction at the exit surface. Walk-off effects can be corrected by compensating crystals [10]. In the monochromatic situation we are considering, Snell's law gives equal exit angles for extraordinary and ordinary

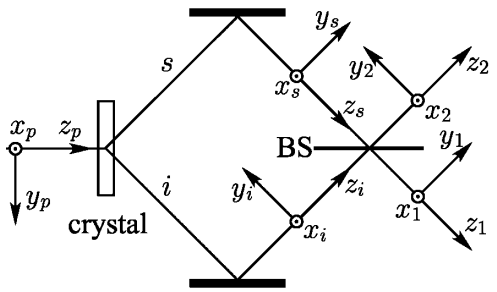

FIG. 1. HOM interferometer. SPDC-created photons are reflected through paths s and i onto a beam splitter (BS). The coordinate systems x_t, y_t, z_t $(t = s, i)$ are transmitted or reflected into coordinate systems x_j, y_j, z_j $(j = 1, 2)$. x_p, y_p, z_p is the coordinate system of the pump field.

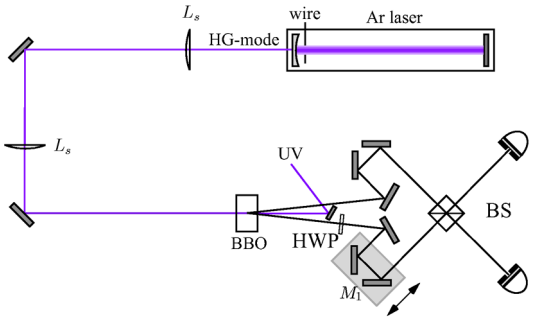

FIG. 2 (color online). Experimental setup. The argon laser is used to pump a BBO (β-BaB_2O_4) crystal cut for degenerate type II phase matching, generating noncollinear entangled photons by SPDC. The wire is used to generate Hermite-Gaussian (HG) modes (see text). The L_s are spherical lenses ($f = 500$ mm) used to focus the pump beam in the plane of the detectors to increase the coincidence detection efficiency [7]. UV is an ultraviolet mirror used to block the laser beam. The down-converted photons are reflected through a system of mirrors and incident on a 50-50 beam splitter BS ($t = r \approx \sqrt{1/2}$). A computer-controlled stepper motor is used to control the path length difference by scanning mirror assembly M_1. HWP is a half-wave plate used to transform the polarization state. The detectors D_1 and D_2 are free space EG&G SPCM 200 photodetectors, equipped with interference filters (1 nm FWHM centered at 702 nm) and 2 mm circular collection apertures. Coincidence and single counts were registered using a personal computer.

polarization. Under these conditions, effects due to the refractive indices and birefringence can be neglected. If the crystal is thin enough, the sinc function in (3) can be considered to be equal to unity [9].

The two-photon detection amplitude, which in the monochromatic case can be regarded as a photonic wave function [11], is

$$\Psi(\mathbf{r}_1, \mathbf{r}_2) = \langle \mathrm{VAC} | \mathbf{E}_2^{(+)}(\mathbf{r}_2) \mathbf{E}_1^{(+)}(\mathbf{r}_1) | \psi \rangle, \tag{4}$$

where $\mathbf{E}_l^{(+)}(\mathbf{r}_l)$ is the field operator for the mode l and $\mathbf{r}_l$ is the detection position. In the paraxial approximation, $\mathbf{E}_l^{(+)}(\mathbf{r})$ is

$$\mathbf{E}_l^{(+)}(\mathbf{r}) = e^{ikz} \sum_\sigma \int d\mathbf{q} \mathbf{a}_l(\mathbf{q}, \sigma) \boldsymbol{\epsilon}_\sigma e^{i[\mathbf{q}\cdot\boldsymbol{\rho} - (q^2/2k)z]}, \tag{5}$$

where k is the magnitude of the wave vector $\mathbf{k}$ and $\boldsymbol{\rho} = x\hat{x} + y\hat{y}$ is the transverse component of the position vector $\mathbf{r} = (x, y, z)$. The operator $\mathbf{a}_l(\mathbf{q}, \sigma)$ annihilates a photon in mode l with transverse wave vector $\mathbf{q}$ and polarization σ.

In the HOM interferometer, the state (2) is incident on a beam splitter. Using the reference frames illustrated in Fig. 1, the annihilation operators in modes 1 and 2 after the beam splitter can be expressed in terms of the operators in modes s and i:

$$\mathbf{a}_1(\mathbf{q}, \sigma) = t\mathbf{a}_s(q_x, q_y, \sigma) + ir\mathbf{a}_i(q_x, -q_y, \sigma), \tag{6}$$

$$\mathbf{a}_2(\mathbf{q}, \sigma) = t\mathbf{a}_i(q_x, q_y, \sigma) + ir\mathbf{a}_s(q_x, -q_y, \sigma), \tag{7}$$

where t and r are, respectively, the transmission and reflection coefficients of the beam splitter. We have assumed that the beam splitter is symmetric. A field reflected from the beam splitter undergoes a reflection in the horizontal (y) direction, while a transmitted field does not suffer any reflection, as illustrated in Fig. 1. The negative sign that appears in the q_y components is due to this reflection. The two-photon wave function is split into four components, according to the four possibilities of transmission and reflection of the two photons:

$$\Psi = \Psi_{tr}(\mathbf{r}_1, \mathbf{r}_1') + \Psi_{rt}(\mathbf{r}_2, \mathbf{r}_2') + \Psi_{tt}(\mathbf{r}_1, \mathbf{r}_2) + \Psi_{rr}(\mathbf{r}_1, \mathbf{r}_2). \tag{8}$$

For convenience, the four components of Ψ are written in two different coordinate systems, $\mathbf{r}_1 = (x_1, y_1, z_1)$ and $\mathbf{r}_2 = (x_2, y_2, z_2)$, since we must work in the paraxial approximation around two different axes z_1 and z_2. To simplify things, we assume that $t = r$. Combining Eqs. (2) through (8), it is straightforward to show that, apart from a common multiplicative factor,

$$\Psi_{tr}(\mathbf{r}_1, \mathbf{r}_1') = i \exp\left\{\frac{iK}{2Z}[(x_1 - x_1')^2 + (y_1 + y_1')^2]\right\}\left[\mathcal{W}\left(\frac{x_1 + x_1'}{2}, \frac{-y_1 + y_1'}{2}, Z\right)\boldsymbol{\Pi}(\boldsymbol{\sigma}_1, \boldsymbol{\sigma}_1') + \mathcal{W}\left(\frac{x_1 + x_1'}{2}, \frac{y_1 - y_1'}{2}, Z\right)\boldsymbol{\Pi}(\boldsymbol{\sigma}_1', \boldsymbol{\sigma}_1)\right], \tag{9}$$

$$\Psi_{rt}(\mathbf{r}_2, \mathbf{r}_2') = i \exp\left\{\frac{iK}{2Z}[(x_2 - x_2')^2 + (y_2 + y_2')^2]\right\}\left[\mathcal{W}\left(\frac{x_2 + x_2'}{2}, \frac{-y_2 + y_2'}{2}, Z\right)\boldsymbol{\Pi}(\boldsymbol{\sigma}_2, \boldsymbol{\sigma}_2') + \mathcal{W}\left(\frac{x_2 + x_2'}{2}, \frac{y_2 - y_2'}{2}, Z\right)\boldsymbol{\Pi}(\boldsymbol{\sigma}_2', \boldsymbol{\sigma}_2)\right], \tag{10}$$

$$\Psi_{tt}(\mathbf{r}_1, \mathbf{r}_2) = \exp\left\{\frac{iK}{2Z}[(x_1 - x_2)^2 + (y_1 - y_2)^2]\right\}\mathcal{W}\left(\frac{x_1 + x_2}{2}, \frac{y_1 + y_2}{2}, Z\right)\boldsymbol{\Pi}(\boldsymbol{\sigma}_1, \boldsymbol{\sigma}_2), \tag{11}$$

$$\Psi_{rr}(\mathbf{r}_1, \mathbf{r}_2) = -\exp\left\{\frac{iK}{2Z}[(x_1 - x_2)^2 + (y_1 - y_2)^2]\right\}\mathcal{W}\left(\frac{x_1 + x_2}{2}, \frac{-y_1 - y_2}{2}, Z\right)\boldsymbol{\Pi}(\boldsymbol{\sigma}_2, \boldsymbol{\sigma}_1), \tag{12}$$

where, for simplicity, we consider $Z = z_1 = z_2$. K is defined just before Eq. (1). $\mathbf{\Pi}(\boldsymbol{\sigma}_1, \boldsymbol{\sigma}_2)$ is the four-dimensional polarization vector of the photon pair. For example, the singlet state in the $H - V$ basis is $\mathbf{\Pi}(\boldsymbol{\sigma}_1, \boldsymbol{\sigma}_2) = 1/\sqrt{2}(\mathbf{H}_1\mathbf{V}_2 - \mathbf{V}_1\mathbf{H}_2)$, where $\mathbf{H}_j$ and $\mathbf{V}_j$ are two-dimensional polarization vectors (for modes $j = 1, 2$) in the horizontal and vertical directions, respectively. $\mathcal{W}(x, y, Z)$ is the transverse field amplitude of the pump beam on the plane $z = Z$, which has been transferred to the two-photon wave function [9]. It is obvious that only $\mathbf{\Psi}_{tt}$ and $\mathbf{\Psi}_{rr}$ can give rise to coincidence detection in D_1 and D_2, while $\mathbf{\Psi}_{tr}$ and $\mathbf{\Psi}_{rt}$ correspond to two photons in arms 1 and 2, respectively.

We now show how $\mathcal{W}$ and $\mathbf{\Pi}$ affect the two-photon interference behavior. Suppose that the photon pair is prepared in a symmetric polarization state: $\mathbf{\Pi}(\boldsymbol{\sigma}_1, \boldsymbol{\sigma}_2) = \mathbf{\Pi}(\boldsymbol{\sigma}_2, \boldsymbol{\sigma}_1)$. If $\mathcal{W}(x, y, Z)$ is an even function with respect to the y coordinate, that is, all the spatial components of $\mathbf{\Psi}$ are symmetric wave functions, then Eqs. (11) and (12) cancel out and there can be no coincidence detections, as is well known [1]. However, if $\mathcal{W}(x, y, Z)$ is an odd function with respect to the y coordinate, direct examination of (9) through (12) shows that (9) and (10) are zero, while (11) and (12) add constructively, resulting in an increase in coincidence counts. Now suppose that the photon pair is prepared in an antisymmetric polarization state: $\mathbf{\Pi}(\boldsymbol{\sigma}_1, \boldsymbol{\sigma}_2) = -\mathbf{\Pi}(\boldsymbol{\sigma}_2, \boldsymbol{\sigma}_1)$. Then for a $\mathcal{W}(x, y, Z)$ that is an even function of y, clearly Eqs. (9) and (10) are zero, while (11) and (12) add constructively, giving a maximum in the coincidence counts. For $\mathcal{W}(x, y, Z)$ that is an odd function of y, (11) and (12) cancel, eliminating coincidence detections.

The behavior of the HOM interferometer for any combination of symmetric and antisymmetric spatial and polarization components of $\mathbf{\Psi}$ can be inferred from the bosonic character of photons, that is, $\mathbf{\Psi}$ must be symmetric.

To our knowledge, all HOM-type experiments performed up until now have used a pump beam that is described by an even function of y. In order to demonstrate experimentally the possibilities of controlling the HOM interferometer with space and polarization variables, we performed a series of experiments in which coincidence counts were registered, combining symmetric and antisymmetric components of $\mathbf{\Psi}$.

A set of beams with well defined Cartesian parity are the HG beams, given by [12]

$$\mathcal{W}_{mn}(x, y, z) = C_{mn}H_m(x\sqrt{2}/w)H_n(y\sqrt{2}/w)e^{-(x^2+y^2)/w^2}e^{-ik(x^2+y^2)/2R}e^{-i(m+n+1)\theta},$$

where C_{mn} is a constant. The $H_n(y)$ are the Hermite polynomials, which are even or odd functions in the y coordinate when the index n is even or odd, respectively. w is the beam waist, $R(z) = (z^2 + z_R^2)/z$, and $\theta(z) = \arctan(z/z_R)$, where z_R is the Rayleigh range.

Pumping the nonlinear crystal with different HG pump beams, we can control the behavior of the down-converted photons at the beam splitter. The experimental setup is a typical HOM interferometer [1], shown in Fig. 2. To generate HG modes we placed a 25 μm diameter wire inside the laser cavity, forcing the laser to operate in one of the HG modes with a nodal line at the position of the wire [12]. The wire is mounted on a rotational stage. We were able to generate first-order modes in any direction ($x, y, \pm 45$, etc.) with laser power $\sim$30 mW. Symmetric and antisymmetric polarization states were used. The symmetric state chosen was $|\Pi^S\rangle = |H\rangle_1|H\rangle_2$ and the antisymmetric state was $|\Pi^A\rangle = (1/\sqrt{2})(|H\rangle_1|V\rangle_2 - |V\rangle_1|H\rangle_2)$, where H and V stand for horizontal and vertical linear polarization, respectively. The state $|\Pi^S\rangle$ was obtained from type II SPDC, by collecting one photon from the ordinary (H-polarized) light cone and the other photon from the extraordinary (V-polarized) light cone followed by a half-wave plate, which rotates its polarization to H. Realigning the crystal, the antisymmetric state $|\Pi^A\rangle$ was obtained from the crossing of the ordinary and extraordinary light cones, followed by compensators, as described in Ref. [10].

Experimental results are sumarized in Figs. 3–5,. The error bars represent statistical errors due to photon counting [11].

Figure 3 shows the results for the symmetric polarization state $|\Pi^S\rangle$ when the crystal is pumped by first-order HG beams $\mathcal{W}_{10}$ and $\mathcal{W}_{01}$. $\mathcal{W}_{10}$, as an even function in y, results in $\mathbf{\Psi}_{rr} = -\mathbf{\Psi}_{tt}$, leading to an interference minimum. $\mathcal{W}_{01}$, as an odd function in y, results in $\mathbf{\Psi}_{rt} = \mathbf{\Psi}_{tr} = 0$ and $\mathbf{\Psi}_{rr} = \mathbf{\Psi}_{tt}$, leading to an

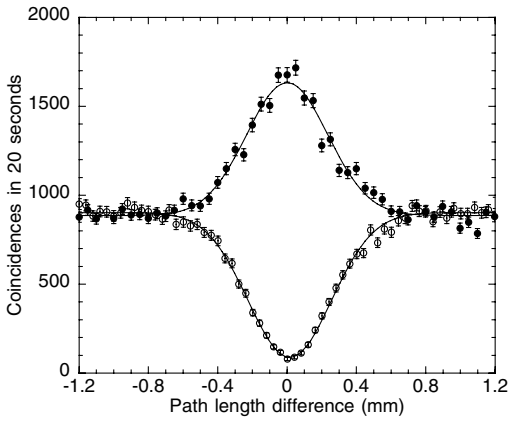

FIG. 3. Coincidence counts when the polarization state is symmetric and the pump beam is a first-order Hermite-Gaussian beam. Open circles (○) correspond to $\mathcal{W}_{10}$ and solid circles (●) correspond to $\mathcal{W}_{01}$.

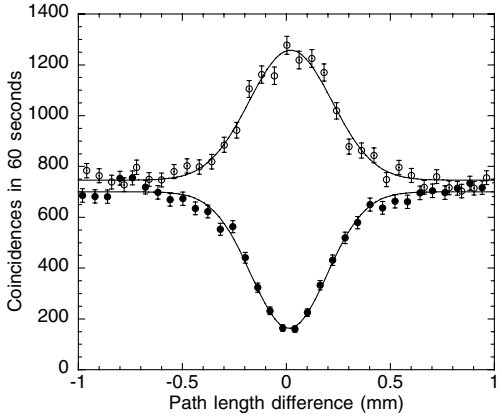

FIG. 4. Coincidence counts when the polarization state is antisymmetric and the pump beam is a first-order Hermite-Gaussian beam. Open circles (○) correspond to $\mathcal{W}_{10}$ and solid circles (●) correspond to $\mathcal{W}_{01}$.

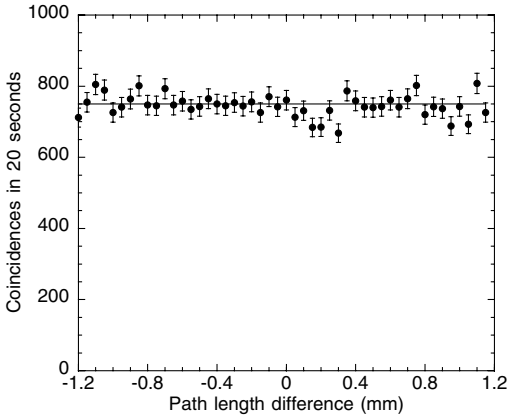

FIG. 5. Coincidence counts when the polarization state is symmetric and the pump beam is an equal superposition of Hermite-Gaussian modes $\mathcal{W}_{01}$ and $\mathcal{W}_{10}$.

interference maximum. The curves have visibilities of 0.90 ± 0.01 ($\mathcal{W}_{10}$) and 0.85 ± 0.01 ($\mathcal{W}_{01}$). Figure 4 shows the results for the antisymmetric polarization state $|\Pi^A\rangle$ under the same pump beam conditions. Now, the behavior of the interference is the opposite, that is, pumping with $\mathcal{W}_{10}$ produces an interference maximum, whereas pumping with $\mathcal{W}_{01}$ produces a minimum. Visibilities of 0.70 ± 0.01 ($\mathcal{W}_{10}$) and 0.77 ± 0.01 ($\mathcal{W}_{01}$) were achieved. Differences in the visibilites were due to the alignment of the interferometer as well as the wire in the laser cavity. We can create an equally weighted superposition of the modes $\mathcal{W}_{01}$ and $\mathcal{W}_{10}$ by placing the wire in the cavity at a 45° angle [12]. Such a superposition is neither symmetric nor antisymmetric. As to be expected, the coincidence count rate is constant, as shown in Fig. 5 for the symmetric polarization state.

We have theoretically and experimentally investigated mulitmode HOM interference using photons generated by SPDC. The resulting interference pattern is seen to depend upon both the transverse amplitude profile of the pump laser and the polarization state of the photon pair. We used first-order Hermite-Gaussian beams to demonstrate that by manipulating the pump beam, one can control the two-photon interference. To our knowledge, this is the first time that two-photon HOM interference has been studied using a spatially antisymmetric wave function.

A possible application of these results is Bell-state analysis without the need for detectors sensitive to photon number [13]. We expect these interference effects to be important in the construction of quantum-optical logic gates [5,6,14], as well as the codification of information in the transverse spatial properties of the photon [15]. In addition, there is the possibility of using these results to create nonclassical states of light with spatial properties that could be useful for quantum imaging.

The authors acknowledge financial support by the Brazilian funding agencies CNPq and CAPES.

*Electronic address: swalborn@fisica.ufmg.br

[1] C. K. Hong, Z. Y. Ou, and L. Mandel, Phys. Rev. Lett. **59**, 2044 (1987).
[2] J. Torgerson, D. Branning, C. Monken, and L. Mandel, Phys. Lett. A **204**, 323 (1995).
[3] K. Mattle, H. Weinfurter, P. G. Kwiat, and A. Zeilinger, Phys. Rev. Lett. **76**, 4656 (1996).
[4] D. Bouwmeester, J. Pan, K. Mattle, M. Eibl, H. Weinfurter, and A. Zeilinger, Nature (London) **390**, 575 (1997).
[5] T. C. Ralph, N. K. Langford, T. B. Bell, and A. G. White, Phys. Rev. A **65**, 062324 (2002).
[6] T. B. Pittman, B. C. Jacobs, and J. D. Franson, Phys. Rev. Lett. **88**, 257902 (2002).
[7] C. H. Monken, P. H. Souto Ribeiro, and S. Pádua, Phys. Rev. A **57**, R2267 (1998).
[8] C. K. Hong and L. Mandel, Phys. Rev. A **31**, 2409 (1985).
[9] C. H. Monken, P. H. Souto Ribeiro, and S. Pádua, Phys. Rev. A **57**, 3123 (1998).
[10] P. G. Kwiat, K. Mattle, H. Weinfurter, A. Zeilinger, A. V. Sergienko, and Y. Shih, Phys. Rev. Lett. **75**, 4337 (1995).
[11] L. Mandel and E. Wolf, *Optical Coherence and Quantum Optics* (Cambridge University Press, New York, 1995).
[12] M. W. Beijersbergen, L. Allen, H. E. L. O. van der Veen, and J. P. Woerdman, Opt. Commun. **96**, 123 (1993).
[13] S. P. Walborn, W. A. T. Nogueira, S. Pádua, and C. H. Monken, Europhys. Lett. **62**, 161 (2003).
[14] E. Knill, R. Laflamme, and G. J. Milburn, Nature (London) **409**, 46 (2001).
[15] J. Leach, M. J. Padgett, S. M. Barnett, S. Franke-Arnold, and J. Courtial, Phys. Rev. Lett. **88**, 257901 (2002).